FUTY Journal of the Environment Vol. 14 No. 1 March, 2020

Analysis of Urban Heat Island of Jos and Environs Using Remotely Sensed Data

*Isioye, O. A., Akomolafe, E. A., Abubakar, A. Z. and Dashe, P.
Department of Geomatics, Ahmadu Bello University, Zaria, Nigeria
*****Correspondence email: lekkyside4u@yahoo.com

Abstract

As a result of the increasing human population especially in the urban areas, and the pressure exacted on land as a result of urbanization, surface temperature is very likely to increase in both frequency and intensity. In most urban areas, this rise in temperature will result to Urban Heat Island (UHI) and this has the potential to negatively influence the health and welfare of urban residents. This study aims at analysing the Urban Heat Island of Jos metropolis and its effect on vegetation and built-up areas. In order to analyse the effects of UHI in the study area, Landsat OLI/TIRS and ETM+ data for the period 2000 – 2018 were utilized in order to retrieve Land Surface Temperature (LST) and the Land Use and Land cover (LULC). The association between LST and Normalized Difference Vegetation Index (NDVI) as well as the Normalized Difference Build-Up Index (NDBI) was also assessed. Results show a weak correlation between LST and NDVI, which corroborates findings from earlier researches that vegetation does influence the formation or otherwise of UHI while there exist a strong correlation between LST and NDBI. This is evident as results indicate that the effect of UHI in Jos is more prominent in compacted built-up areas compared to the surrounding rural areas. The UHI effect from Landsat data shows an average increase of 6.75^{o}C in surface temperature between 2000 and 2018. The study recommends that increased vegetation should be encouraged in the study area to reduce the effect of UHI.

Keywords: LST, UHI, NDVI, NDBI, Landsat OLI, TIRS, ETM+

INTRODUCTION

A typical phenomenon of urban climates that challenge viable livelihoods in cities is Urban Heat Island (UHI) which describes the excess temperature near the ground (canopy layer) of the central urban locations as being higher than those of nearby or surrounding areas of similar elevation (Voogt, 2003). The temperature difference usually is larger at night than during the day and is most apparent when winds are weak. The UHI has been regarded as the well-documented example of anthropogenic climate modification within the field of urban climate (Arnfield, 2003).

According to Adam (2009), the main contributor to UHI is the properties affecting heat retention and transfer from urban surfaces to the cooling atmosphere in the evening. Urban material properties cause surfaces exposed to sunlight to attain high land surface temperatures (LST). Urban surfaces absorb and retain solar radiation during clear and sunny days. Irradiated

urban surfaces then transfer the stored heat energy to the near surface air (boundary layers) by radiation and conduction throughout the evening.

The main cause of UHI include modification of land surfaces as a result of rapid urbanization. This urban population, in order to be accommodated has led to an increase in the number of high-rise structures which also uses materials that effectively retain heat. Growth in the vertical dimension influences wind flow within the urban area, which is a key microclimate phenomenon because it counteracts UHI effect and also disperses the accumulated pollution (Jhaldiyal, 2015). Land cover types that contribute to increased heat retention include pavement, rooftops, sidewalks, roads, and parking lots (Adebayo *et al.,* 2017).

Cities have a warmer climate than rural areas due to the UHI, which represents one of the most significant human-induced changes to earth's surface climate (Zhou *et al.*, 2004). UHI effect also impacts on the development of meteorological events such as increased precipitation, boosts energy demands, poses threats to environmental quality and long-term sustainability of localities and these potentially contributes to global warming (Kikegawa, 2006).

Studies have shown a relationship between UHIs and patterns of land cover changes. Results from some of these studies show that the presence of vegetation and water lessened the intensity of UHIs (Chen *et al.*, 2006; Amiri *et al.*, 2009; Sun *et al.*, 2012; Igor and Vanessa, 2012). In Igor and Vanessa (2012), the change in the land cover patterns were analysed quantitatively according to their relationship with the LST. To quantify these changes, Land use indices such as the Normalized Difference Vegetation Index (NDVI), Normalized Built-up Index (NDBI) and Land use land cover map (LULC) were used.

As urbanization is accelerating across the world, especially in developing countries, the UHI effect has gained importance to be investigated (Kalnay and Cai, 2003). The pattern, trend and characteristics of urbanization in Nigeria has been on the rise as urban sprawl has been observed in various cities across the country (Olujimi, 2009; Ujoh *et al*., 2010; Avis 2019). Town and cities have grown unbelievably with the pace of urbanization in Nigeria showing high growth rates of 5% - 10% per annum (Egunjobi, 2009). Consequently, there has been a rapid expansion of Nigerian cities, up to 10 times their initial point of growth (Agbola and Agbola, 1997). Several studies have shown that inadequate planning of urban land in Nigeria and great intensity of use has aggravated urban problems, one of which is the UHI (Egunjobi, 2002; Isioye *et al.*, 2019).

With the accelerated rate of urbanization, UHI has become more and more significant and has had a severe impact on urban development and human living environment (Chen *et al.*, 2009). Meanwhile, increasing urban heat in Nigerian cities presents a significant health risk for the growing population and the related heat stress is likely to escalate with the increase in temperature as projected (Osborn, 2016; World Bank Group, 2020). It is against this

background that this research seeks to use remotely sensed surface temperature data to analyse the urban heat island in Jos and its environ and to find potential mitigation strategies that will facilitate adaptation to new environmental conditions. It also seeks to analyse the relationship between UHI phenomena, NDVI, NDBI and LULC in the study area using a quantitative approach. This study spatio-temporally investigated the UHI using LST derived from Landsat data between the years 2000 and 2018 over the study area.

METHODOLOGY

Study area

The study area is the city of Jos and its environ. Geographically, it is located between latitudes 8°55′ to 10°11′ North of the equator and longitudes 8°21′ and 9°30′ East of the central meridian, with a total area of about 8,600 km^2. The population of the study area is estimated to be about 900,000 (UN, 2019). It consists of Jos North, Jos East and Jos South Local Government Areas (LGAs). According to (Nanzip, 2020), the study area has a tropical climate with an average annual rainfall of about 1,324mm. It also has a temperate climate with its temperature lower than that of most cities in Nigeria because of its high altitude with average monthly temperature ranging between 21ºC and 25℃ for all the months.

From mid-November to late February, night time temperature drops as low as 11℃ while day time temperature may remain in the range 14℃ to 19℃. Its topography is characterized by a rugged terrain consisting of rocks, hills and valleys and it is home to many tourist sites. The population growth rate in Jos metropolis increased from 14% in 1900 to 50.5% in 2010 (Seifolddini and Mansourian, 2014). The unprecedented population growth coupled with developmental activities such as tin mining has led to urbanization (Adzandeh, 2015). A map of the study area is shown in the Figure 1.

Data

Cloud-free Landsat 7 ETM+ and Landsat 8 OLI were obtained from the USGS website and were processed in order to generate land use/cover changes (LULC) maps, retrieve LST, detect the changes in UHI in the area under study and to compute various indices. The details of the Landsat images selected for this study are presented in Table 1. Landsat data are frequently used for land-use and land-cover change analyses (Yuan *et al.,* 2005; Bagan *et al.,* 2010) and are useful for deriving the surface temperature (Kumar *et al.,* 2012). The Landsat images were all subsequently subjected to radiometric calibration to produce scaled and comparable data and to reduce scene-to-scene variability (Chander *et al.,* 2009). Radiometric calibration is a multi-step process that involved the use of standard equations to convert 8-bit satellite quantized calibrated digital numbers (DN) to satellite reflectance.

Image correction and processing

Geometric correction was carried out on all Landsat images as they were converted into the same projected coordinate system (UTM Zone 32N on WGS84 ellipsoid) to analyse the changes in LULC, LST, NDVI and NDBI in the study area. In this study, the software ENVI

5.3 and ArcGIS 10.3 were used for image pre-processing, processing and spatial analysis. Furthermore, the scan line error of Landsat 7 images of year 2006 and 2012 was removed using Landsat gap-fill tool in ENVI environment. A study area covering approximately 1,780km^2 was extracted as a subset from the Landsat full scene images. Then false colour images were created for visual interpretation and in order to perform correct image classification.

Table 1. Details of the Landsat data used.

S/no.	Satellite	Sensor	Path/Row	Acquisition date	Spatial resolution of Spectral and TIR bands
1	Landsat 7	ETM+	188/53	04/03/2000	30m/60m
2	Landsat 7	ETM+	188/53	22/04/2006	30m/60m
3	Landsat 7	ETM+	188/53	23/03/2012	30m/60m
4	Landsat 8	OLI/TIRS	188/53	14/03/2018	30m/100m

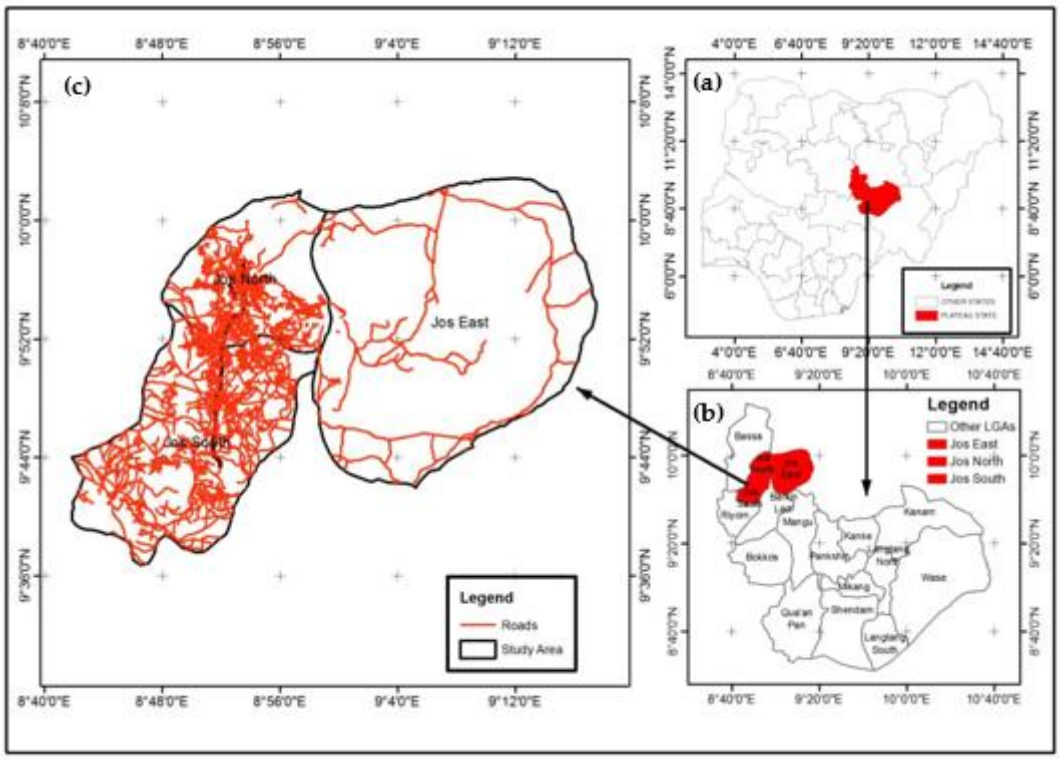

Figure 1. Map of the study area, (a) Plateau state in northern Nigeria; (b) Local government areas in Plateau state and locational position of Jos; (c) Jos Township comprising of Jos North, Jos South and Jos East.

Retrieval of Land Surface Temperature (LST)

Landsat 7 (ETM+) band 6 (10.4 – 12.5µm) and Landsat 8 (OLI/TIRS) band 10 (10.60 - 11.19µm) are considered suitable as shown by many literatures for capturing the multifaceted intra-urban temperature differences thus makes it effective for urban climate analysis (Adebayo *et al.*, 2017). In this study, the data used to estimate the LST were acquired for the months of March and April (when the temperature is relatively high).

Conversion of DN to spectral radiance

To retrieve the LST, the Landsat data were first radiometrically corrected by converting the digital numbers (DN) of each band to spectral radiance. It has been proven that radiation correction improves the accuracy of LST and other index calculation (Song *et al.*, 2001). This was achieved in ENVI software using the following equation (Landsat Project Science Office, 2002; 2016):

$$L_\lambda = M_L \times QCal + A_L, \quad (1)$$

equation (1) can be rewritten as:

$$L_\lambda = \frac{L\max_\lambda - L\min_\lambda}{(QCal_{max} - QCal_{min})} \times (QCal_{max} - QCal_{min}) + L\min_\lambda \quad (2)$$

In equations (1) and (2), L_λ is TOA spectral radiance in Watt/(m^2srμm), M_L is the band-specific multiplicative rescaling factor from the metadata (RADIANCE_MULT_BAND 6 for Landsat 7 ETM+, while BAND 10 is for Landsat 8 OLI/TIRS), QCal is the quantized and standard product pixel value (DN), A_L is the band-specific additive rescaling factor from the metadata (RADIANCE_ADD_BAND 6 for Landsat 7 ETM+, while BAND 10 is for Landsat 8 OLI/TIRS), $Qcal_{max}$ = 255 ($Qcal_{max}$ is the maximum number of each band), $Qcal_{min}$ = 1 ($Qcal_{min}$ is the minimum number of each band), and Lmax and Lmin are spectral radiance for thermal bands at DN 255 and 1, respectively in Watt/m^2 sr μm.

Conversion of spectral radiance to TOA brightness temperature

The spectral radiance converted from pixel DN values above was then used to compute Top of Atmosphere brightness temperature (T_B) which is the effective temperature viewed by the satellite under an assumption of unit emissivity in Kelvin. The brightness temperature was computed using the following equation:

$$T_B = \frac{K_2}{ln\left(\frac{K_1}{L_\lambda} + 1\right)} \quad (3)$$

In equation (3), K_1 and K_2 = band specific thermal conversion constant. For Landsat 7 ETM+, K_1 = 666.09 mW/cm^2/sr/μm and K_2 = 1282.71 Kelvin; for Landsat 8 OLI, K_1 = 774.89 mW/cm^2/sr/μm and K_2 = 1321.08 Kelvin

Derivation of NDVI and NDBI

The Normalized Difference Vegetation Index (NDVI) is a measurement of the amount and vigour of vegetation at the surface. NDVI values rages from -1 to +1. The index is defined by the equations (4a and b).

$$NDVI = \frac{NIR - RED}{NIR + RED} \quad (4a)$$

In equation (4a), NIR and RED in Landsat 7 ETM+ are the reflectance in the near-infrared (band 4) and red (band 3) portion of Electromagnetic spectrum respectively. For Landsat 8 OLI/TIRS, the NDVI is contained in equation (4b);

$$NDVI = \frac{Band5 - Band4}{Band5 + Band4} \tag{4b}$$

In the equation (4b), Band 5 and Band 4 are the reflectance bands in the near-infrared and red portion of Electromagnetic spectrum of Operation Land Imager (OLI) sensor of Landsat 8 respectively (Adebayo *et al.*, 2017).

The NDBI (Zha *et al.*, 2005) was introduced in this study to detect built-up areas. The Normalized Difference Built-up Index (NDBI) is derived from Landsat ETM+ and OLI/TIRS data, using equations (5a) and (5b) respectively.

$$NDBI = \frac{Band4 - Band5}{Band4 + Band5} \tag{5a}$$

$$NDBI = \frac{Band6 - Band5}{Band6 + Band5} \tag{5b}$$

Estimation of proportion of vegetation and emissivity

Land surface emissivity (LSE) can be derived from the emitted radiance measured from space. Land surface emissivity is the average emissivity of an element of the surface of the Earth calculated from NDVI values. The proportion of vegetation (Pv) is computed as follows:

$$Pv = \left[\frac{(NDVI - NDV\,Im\,i\,n)}{(NDV\,Im\,a\,x - NDV\,Im\,i\,n)}\right]^2 \tag{6}$$

Where, *Pv* = Proportion of vegetation, NDVI = NDVI Values from the Image, NDVImin = Minimum NDVI, and NDVImax = Maximum NDVI. Using the computed value of proportion of vegetation (Pv) the Land Surface Emissivity (e) was computed as follows:

$$e = 0.004 * P_v + 0.986 \tag{7}$$

Land Surface Temperature (LST) retrieval

The following equation were used for the conversion from at-satellite temperature to land surface temperature in Celsius. $LST = \frac{T_B}{\left[1+\left(\lambda\times\frac{T_B}{\rho}\right)ln(e)\right]}$ (8)

$$LST(^oC) = LST(K) - 273.15 \tag{9}$$

In equation (9), λ is the wavelength of emitted radiance, ρ = h×(c/s) = 1.4388 × 10^{-2}m K = 14388 μm K, h is the plank's constant = 6.626 × 10^{-34}Js, s is the Boltzmann constant = 1.38

$\times 10^{-23}$J/K, c = velocity of light = $2.998 \times 10^{8} m/s$. The value of λ for Landsat bands are listed in Table 2.

Table 2. Wavelength value for Landsat Satellites

Satellite	Band	Middle λ (μm)
Landsat 4, 5 and 7	6	11.45
Landsat 8	10	10.8

Image classification and accuracy assessment

In order to detect LULC changes in the study area and to investigate their relationships with the spatial patterns of LST and indices (NDVI, NBDI), visible (Red, Blue, Green) and near-infrared bands of the Landsat images were used for supervised classification of the LULC types in the study area using a Maximum Likelihood algorithm. Accordingly, the LULC types were categorized into four classes, namely: built-up, water body, vegetation and bare surface using ArcGIS 10.3 software. In the classification, the exposed rocks and uncultivated land were combined as bare surface. The land use classes identified were selected as they have been reported to exhibit specific characteristics in terms of surface temperature (Amiri *et al.*, 2009; Chen *et al.*, 2006; Li *et al.*, 2012). Before the supervised classification of images was applied, training data were carefully chosen for all four classes by visual interpretation.

The accuracy assessment of the classification was performed using the computed error matrix. Error matrix was obtained by collecting data for every class without seeing the segments and classes. Eventually, the areas related to uses in all years under study were extracted after controlling the classification accuracy and confirming the meaningfulness of the errors. The Overall Accuracy and Kappa Coefficient were calculated to assess the accuracy of the classification results. To recognize changes during the studied period, classified images were compared. Overall accuracy is the simplest and most popular of the accuracy measures and is computed by dividing the total correct by the total number of pixels in the error matrix. Kappa coefficient gives an adequate accuracy measure in the thematic classification for representing class accuracy.

RESULTS AND DISCUSSION

Land Use/Cover Changes

The land use land cover maps for the year 2000, 2006, 2012 and 2018 were generated from supervised classification as seen in Figure 2.

The area occupied by each Land use/Land Cover class was also estimated and are presented in Table 3. In this study, the total area of the study area is estimated to be 1780.13km^2. The results indicate that the percentage of area under different land use classes have drastically changed in the last 20 years, from 1998 to 2018.

Table 3. Area statistics of LULC classes in the study area for years under study

LULC Classes	2000		2006		2012		2018	
	Area of LULC		Area of LULC		Area of LULC		Area of LULC	
	km^2	%	km^2	%	km^2	%	km^2	%
Built-up	332.07	18.65	379.11	21.30	426.66	23.97	551.98	31.01
Water body	7.14	0.41	18.53	1.04	8.27	0.46	8.40	0.47
Vegetation	159.21	8.94	193.83	10.89	189.15	10.63	221.80	12.46
Bare surface	1281.71	72.00	1188.66	66.77	1156.05	64.94	997.96	56.06
Total	1780.13	100	1780.13	100	1780.13	100	1780.13	100

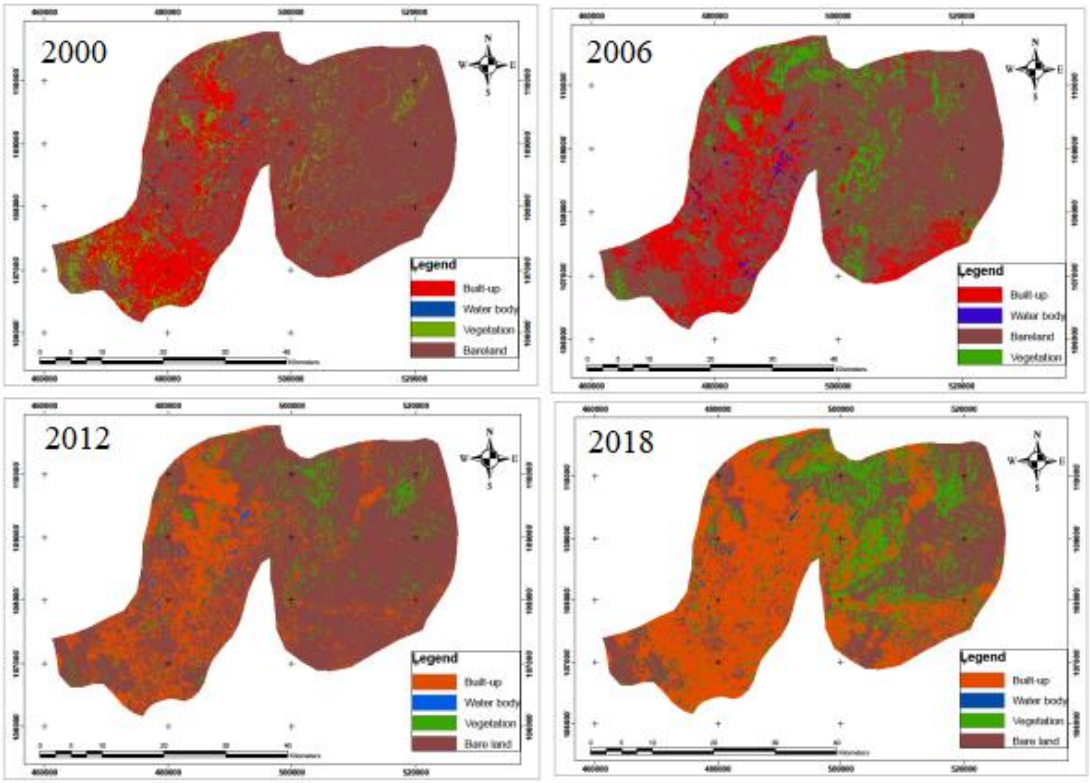

Figure 2. Results of Land use land cover classification for the year 2000, 2006, 2012 and 2018.

Results show that the total built-up area has increased from 18.65% (332.07km^2) of the total land area in 2000 to 21.30% (379.11km^2) in 2006, a 2.65% increment. However, water body in the study area increased to 1.04% (18.53km^2) in 2006 from 0.41% (7.14km^2) in the year 2000, an increase of 0.63% while vegetation increased from 8.94% (159.21km^2) to 10.89 (193.83km^2), a 1.95% increase within the same period. Built-up area which covers the largest area in the study area on the other hand decreased by 5.23% from 72.00% (1281.71km^2) to 66.77% (1188.66 km^2) between the years 2000 and 2006.

In 2012, built up area increased by 2.67% from 21.30% (379.11km^2) in 2006 to 23.97% (426.66km^2). Water body, vegetation and bare surface on the other hand decreased by 10.26%, 4.68% and 32.61% respectively between 2006 and 2012 (see Table 4) with corresponding areal values of 8.27km^2, 189.15km^2 and 1156.05km^2 (see Table 3).

Furthermore, between 2012 and 2018, the built-up area gained more increment of 12.36%, with a value of 31.01% (551.98km^2) from 23.97% (426.66km^2) of the total LULC in 2012. Water body and vegetation both gained 0.01% and 1.83% respectively, amounting to 0.47% (8.40km^2) and 12.46% (221.80km^2). The dominant land cover; bare surface in the study area appeared to have reduced drastically in 2018 by 8.88% (see Table 4) amounting to 56.06% (997.96km^2) of the total LULC (see Table 3). Figure 3 shows the resulting land use/ land cover maps, while the Tables 4 depicts the area covered by land use and land cover classes and the rate of change of the classes.

Table 4. LULC changes between 2000 and 2018.

	2000 – 2006		2006 – 2012		2012 – 2018		2000 – 2018	
LULC Classes	Area (km^2)	%	Area (km^2)	%	Area (km^2)	%	Area (km^2)	%
Built-up	47.04	2.65	47.55	2.67	125.32	7.04	219.91	12.36
Water body	11.39	0.63	-10.26	-0.58	0.13	0.01	1.26	0.06
Vegetation	34.62	1.95	-4.68	-0.26	32.65	1.83	62.59	3.52
Bare surface	-93.05	-5.23	-32.61	-1.83	-158.09	-8.88	-283.75	-15.94

Generally, as seen in Figure 3, results show that the total built-up area increased from 18.65% of the total land area in 2000 to 31.01% in 2018, an increase of 12.36% over the period of 18 years. It was observed that the built-up area has significantly increased in the city center and its environs.

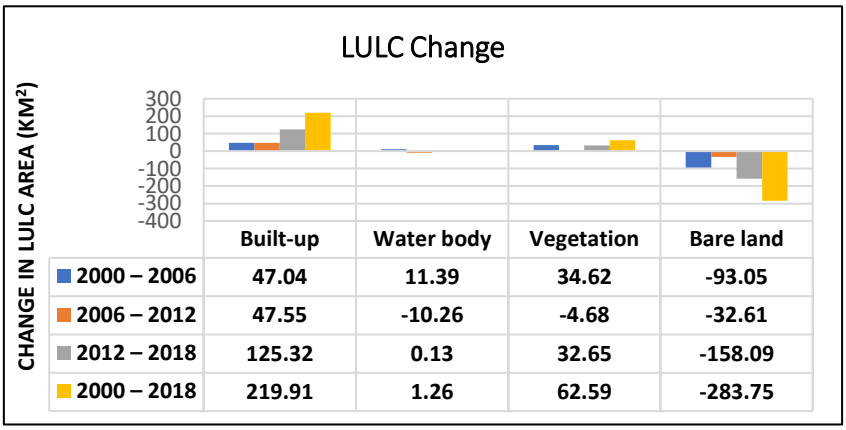

Figure 3. LULC change within the study area.

Population growth and rapid urbanization has been the major cause for the built-up land use increment. Bare surface appears to be the predominant land cover type in the area under study though it reduced drastically from what was obtainable in 2000 and what we see in 2018. This is attributed to open surfaces being converted to be used for residential purposes as the population grows.

Result of accuracy assessment

Segments of the four LULC classes considered in this study were chosen from the original Landsat images. The error matrix was obtained by collecting data for every class without seeing the segments and classes. The accuracy parameters were calculated and evaluated with the help of the error matrix. The overall accuracy assessment of the supervised classification is presented in Table 5 for all classes of different years.

Table 5. Accuracy assessment of the classified images.

LULC Classes	2000		2006		2012		2018	
	Producer's Accuracy (%)	User's Accuracy (%)	Producer's Accuracy (%)	User's Accuracy (%)	Producer's Accuracy (%)	User's Accuracy (%)	Producer's Accuracy (%)	User's Accuracy (%)
Built-up	92.5	100	97.5	97.5	100	100	95.5	90.5
Water body	97.5	95.1	100	100	100	97.5	100	97.5
Vegetation	100	90.9	97.5	97.5	100	100	92.5	100
Bare surface	95.0	100	100	100	97.5	100	97.5	95.1
Overall Accuracy	**96**		**98**		**97**		**90**	
Kappa Statistics	0.86		0.89		0.89		0.85	

The kappa coefficient measures the agreement between classification and truth values. A kappa value of 1 represents perfect agreement, while a value of 0 represents no agreement. Therefore, the closer the kappa coefficient is to 1, the higher the classification accuracy and its acceptability (Bharatkar and Patel, 2013). A Kappa coefficient of 0.90 may be interpreted as 90% better classification than would be expected by random assignment of classes. The general range for Kappa values are if $K < 0.4$, a poor kappa value; while, if $0.4 < K < 0.75$, is a good kappa value and if $K > 0.75$, it is an excellent kappa value (Vieira *et al.*, 2010; Bharatkar and Patel, 2013).

Results as seen in Table 5 show overall accuracies of 96%, 98%, 97% and 90% and Kappa coefficients of 0.86, 0.89, 0.89 and 0.89 for the year 2000, 2006, 2012 and 2018 respectively for the image classification. These values are interpreted as excellent image classification for each year.

Spatial pattern of LST in Jos metropolis

LST provides relevant information about the surface physical properties and climate which plays a significant role in many environmental processes. Figure 4 shows the spatial distribution of LST in the study area between 2000 and 2018.

The LST maps above show the spatial distribution of day-time LST in the Jos metropolis and environs in 2000, 2006, 2012 and 2018. In 2000, LST ranged from 11.98^{o}C to 29.60^{o}C across the city. However, in 2006 and 2012, the LST slightly increased and ranged from 13.86^{o}C to

31.02ºC and 14.17ºC to 31.40ºC respectively. It was also observed that there was a slight increase in LST in 2018 ranging from 16.06ºC to 38.98ºC.

Highest temperatures were observed in the city center which is located south-west of the study area. Other location experiencing high temperatures as seen in Figure 4, is the south-east of the region and other built-up areas which have increased between 2000 and 2018 as seen and discussed in preceding section of this report. However, it was observed that in the study area, the there was little expansion in built up land use within the city center as compared to surrounding rural areas which has experienced expansion and urban sprawl over the years. This among other factors such as topography, cost of living, nature of materials uses for building and also clearing of vegetation has led to the increase in the temperature of the surrounding areas of the metropolis against the usual perception that the urban areas is an island of heat amidst its surrounding rural areas.

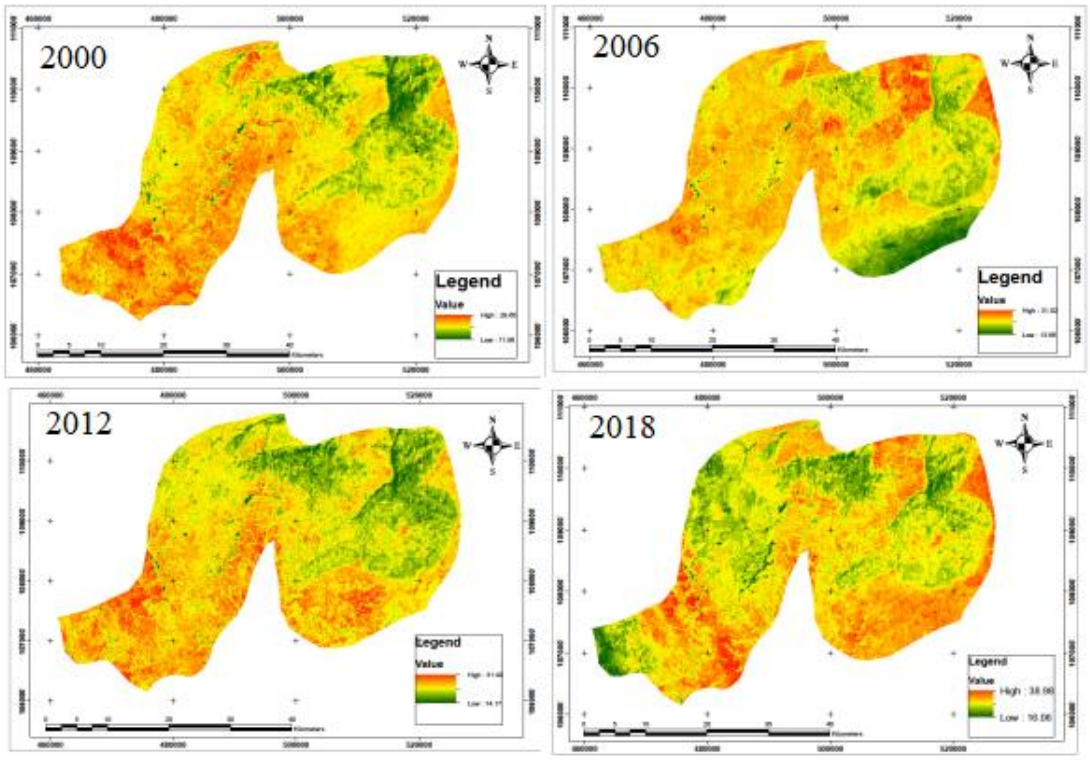

Figure 4. LST distribution of Jos metropolis and environ in 2000, 2006, 2012 and 2018.

Evaluation of Urban Heat Island

The Urban Heat Island (UHI) effect is a phenomenon where the urban temperature is higher than the surrounding rural environment temperature (Oke, 1982). In order to validate these assumptions, the results from the generated maps (LULC and LST) and the graphs were analysed. The four classified images which show the urban sprawl in Jos were taken into account in order to select points from which the LST were recorded. In this study the UHI phenomena was also analysed based on the temperature change per year within the study

period. It was observed how temperature changes consistently as built-up area expands. The average temperature for the year 2000 was observed to be 20.79℃ with 332.07km^2 being occupied by built-up area. In the year 2006 and 2012 the changes in temperature and built-up areas were not very large. The average temperature was 22.44℃ and 22.79℃ respectively while the built-up area occupied 379.11km^2 and 426.66km^2 of the total study area respectively. It was recorded that there was a rapid increase in built-up area and raise in temperature in the year 2018. The average temperature was recorded as 27.52℃ with the built-up area taking 551.98km^2 of the total land mass.

Therefore, spatio-temporally, results show that Jos metropolis and environ experienced UHI especially within the built-up area as temperature increased over a span of 18 years between 2000 and 2018.

Vegetation distribution

As opined by Adebayo (2017), NDVI is a measure of the vegetation density of an area and tends to reduce with increase in the alteration of natural surfaces and replacing them with impervious surfaces. The distribution of vegetation within the study area was analysed using the NDVI. Figure 5 shows the NDVI in the study site between 2000 and 2018.

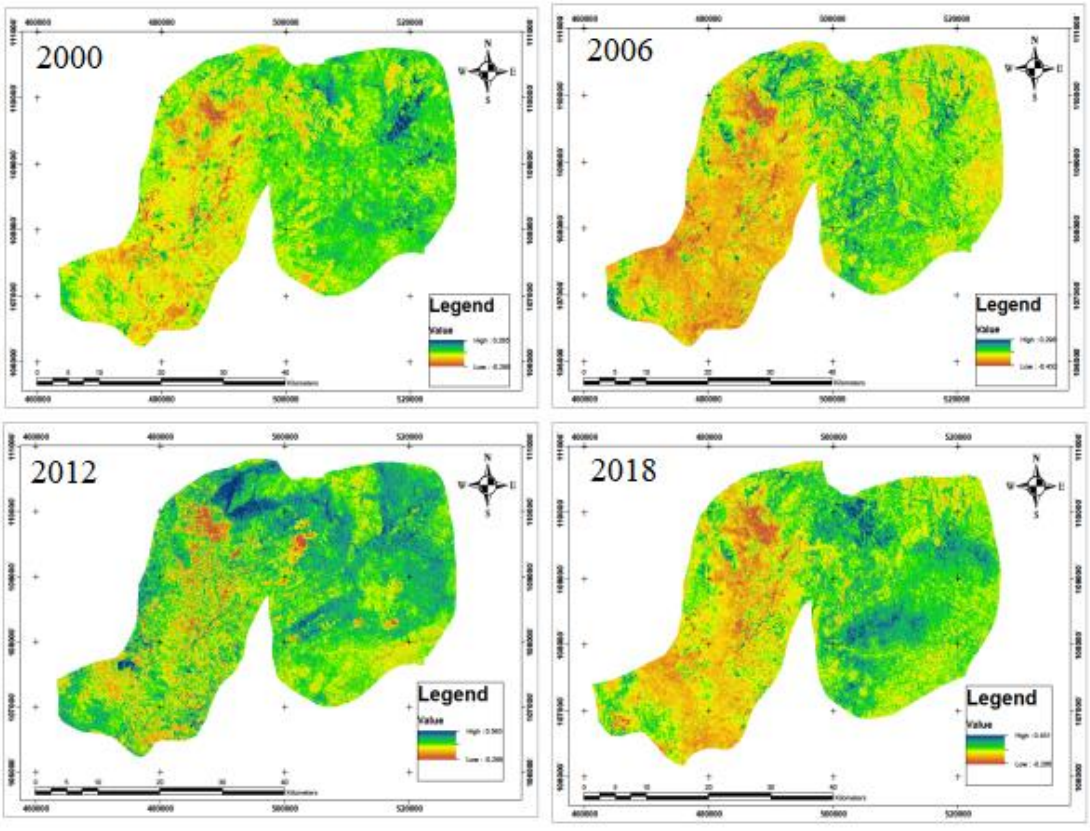

Figure 5. NDVI distribution of Jos metropolis and environs

NDVI maps were generated for the years 2000, 2006, 2012 and 2018 in order to estimate the vegetation abundance, using Red and NIR bands of Landsat 7 and Landsat 8. The high NDVI

values indicate abundance of vegetation as compared to areas with low NDVI values (see Figure 5). The value of NDVI in 2000 ranged from -0.295 to 0.285 while that of year 2006 was observed to have a range of values from -0.432 to 0.296 which is slightly higher than that of 2000. Similarly, it was observed that the NDVI values for the year 2012 ranges from -0.267 to 0.594 and finally, that of the year 2018 were observed to have a range of values from -0.266 to 0.431 which is lower compared to 2012. The NDVI value as shown in Figure 5 revealed that lower NDVI is associated with the developed settlements, rocks and bare surfaces while high NDVI values is associated with the less developed natural surfaces.

Relationship between LST and Land Use Land Cover

The LULC maps were overlaid with the corresponding LST map for each year under study in ArcGIS 10.3 environment. In addition, fifteen (15) sample points were generated for each class (Built-up, Water body, Vegetation, and Bare surface) and the corresponding LST value was generated using the "extract multiple values to points" tool. Line graphs were generated from these values to show the temperature associated with each LULC per year as shown in Figure 6. Points generated from built-up class were selected from the city center so as to represent the urban temperature while vegetation and bare surface class were assumed to represent rural temperature.

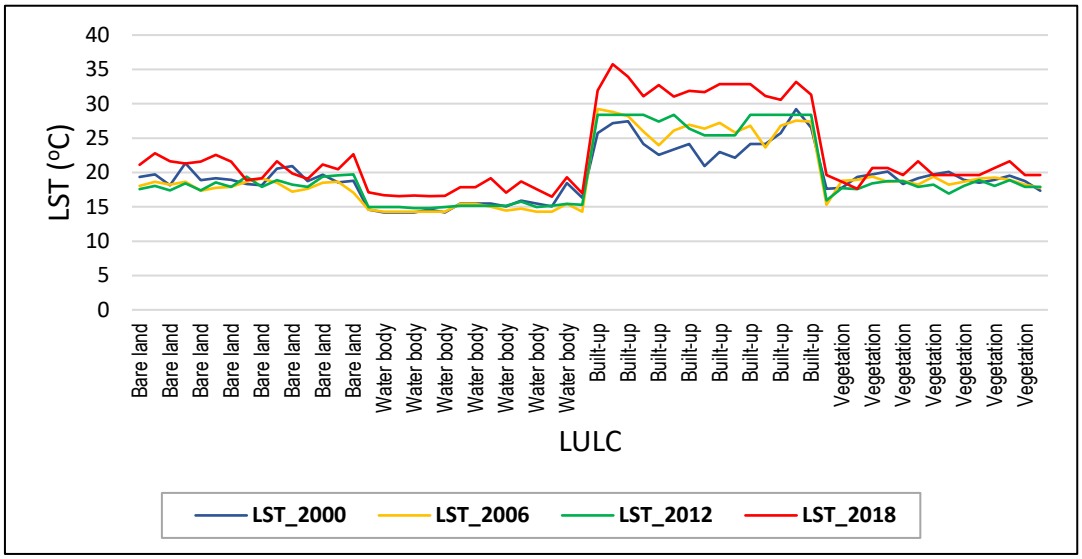

Figure 6. Relationship between LST and LULC in 2000, 2016, 2012 and 2018

It was observed that high temperatures are present in the built-up areas and bare surfaces while vegetation and water bodies show lower temperatures. It can be deduced that the high temperatures recorded in the built up and bare surfaces is as a result of anthropogenic activities and urbanization. More open spaces are being converted for residential use and some of these surfaces are also exposed, devoid of vegetation thus, retaining heat. It is also observed as seen from Figure 6 that in the built-up area, there is an increase in LST between 2000 and 2018. This corroborates results obtained earlier in the distribution of LST in the study area.

Relationship between LST, NDVI and NDBI

Using XLSTAT; an add-in to Microsoft Excel, the relationship between the NDVI, NDBI and the LST was established to test the correlation between these variables. This was achieved by running a regression analysis. Results are presented below.

From the results obtained as seen in Figure 7, it was observed that there exists a weak negative correlation between LST and NDVI with Pearson correlation coefficient values of R = 0.3153, 0.167, 0.1749, 0.3312 for the years 2000, 2006, 2012 and 2018 respectively, all at 95% confidence interval. This implies that the presence of vegetation has an influence on the value of LST obtainable at a particular location and it can be said that, where vegetation exists, the temperature of that area is less compared to a built environment. The relationship between LST and NDBI is shown in Figure 8.

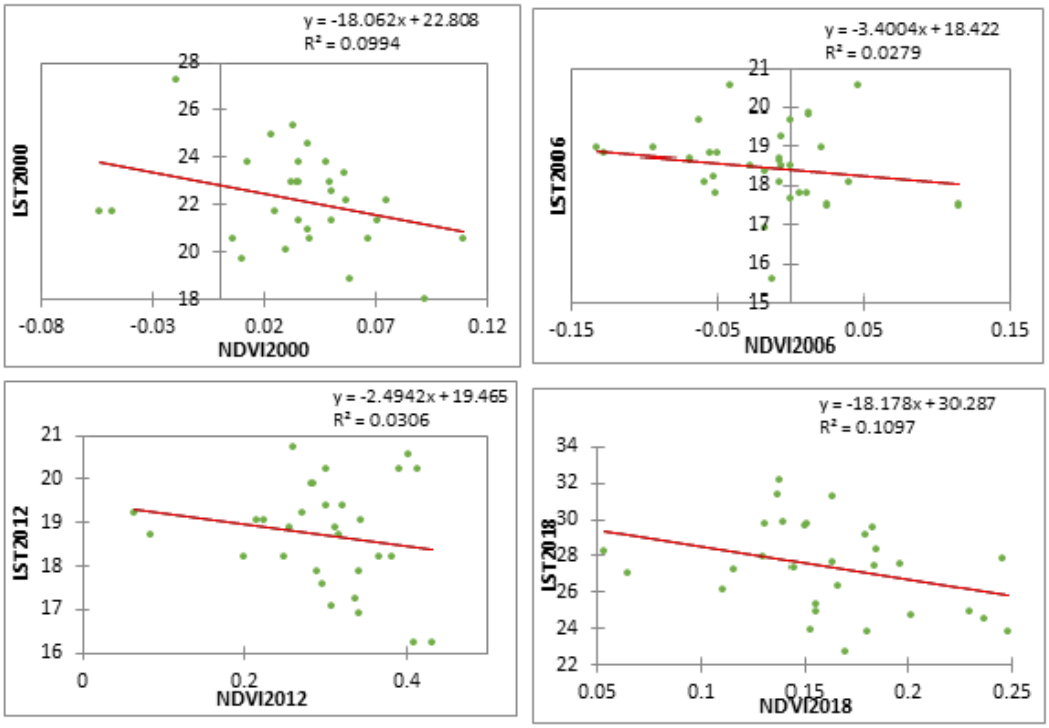

Figure 7. Relationship between LST and NDVI in 2000, 2016, 2012 and 2018.

Results show that there is a strong positive correlation between LST and NDBI for the years for the years 2000, 2006, 2012 and 2018 at 95% confidence interval as seen in Figure 8. The implication is that the value of LST increases as the built-up area increases thus giving rise to UHI as the city is urbanized over time.

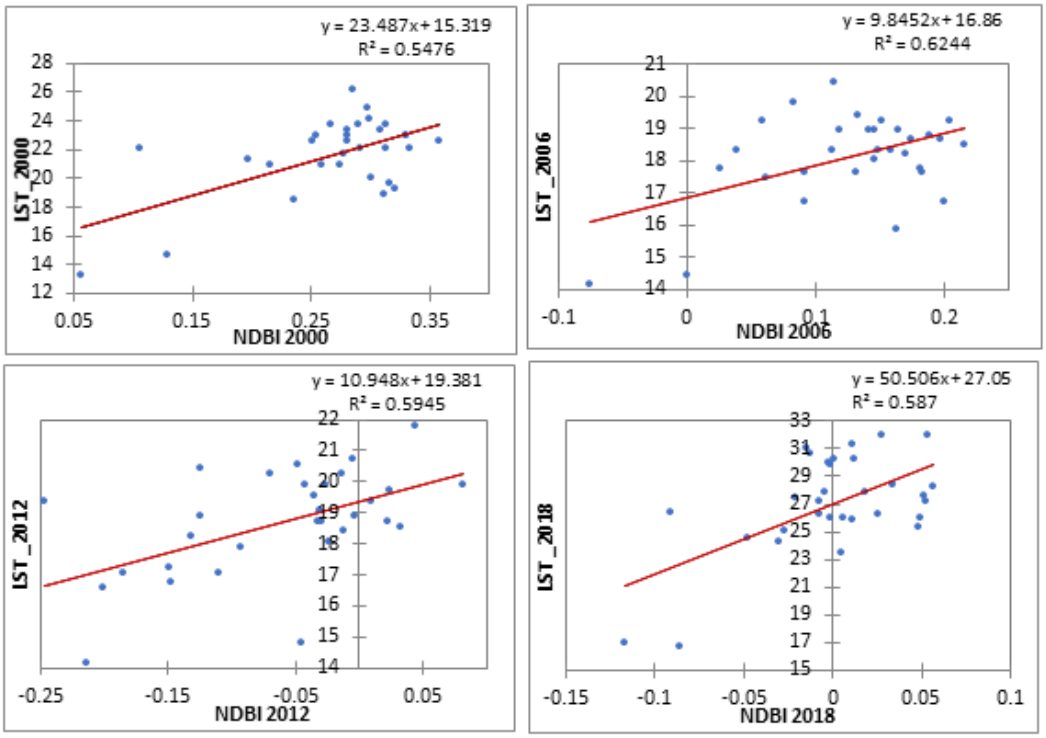

Figure 8. Relationship between LST and NDBI in 2000, 206, 2012 and 2018

CONCLUSIONS

From the study it has been seen that from the year 2000 to the year 2018, the temperature of Jos is significantly increasing as no period share the same average temperature. From the findings, it can be stated that, the increased in temperature maybe as a result of increased in built-up and very little presence of water bodies. In this study, the split-window algorithm was applied to retrieve the LST in Jos using the Landsat ETM+ and Landsat OLI/TIRS data to study the concept of UHI in that region. From the correlation between LST and NDVI, it was concluded that, NDVI can be a measure control of LST, because increase in vegetation will decrease temperature and vice versa. Meanwhile, a strong correlation exists between the NDBI and LST as correlation it indicating an increase in LST as the built-up area increases. It is inevitable to avoid development in the cities, but cities can be planned in such a way that urbanization should have less effect especially on heat stress. Urban planners should engage in extensive decongestion of the crowded parts of our cities, so as to avoid heat stress and tree planting and cultivation should be encouraged to mitigate against UHI in Jos metropolis.

References

Adam, L. B. (2009). Temperature Trends and Urban Heat Island Intensity Mapping of the Las Vegas Valley Area. Master of Science in Civil Engineering, University of Nevada, Las Vegas, 2009. A thesis submitted in partial fulfilment of the requirements for the Master of Science in Engineering.

Adebayo, F. F., Balogun, I. A., Adediji, A. T., Akande, O. and Abdulkareem, S. B. (2017). Assessment of Urban Heat Island over Ibadan Metropolis Using Landsat and MODIS. *International Journal of Environment and Bioenergy, 12(1):*62-87, ISSN: 2165-8951.

Adzandeh, E. A., Akintunde, J. A. and Akintunde, E. A. (2015). Analysis of Urban Growth Agents in Jos metropolis, Nigeria. *International Journal for Remote Sensing and GIS, 4(2):* 41-50, ISSN 2277-9051.

Agbola, T. and Agbola, E. O. (1997). The Development of Urban and Regional Planning Legislation and their Impact on the Morphology of Nigerian Cities. *Nig. J Econ. Soc. Stud., 39(1):* 123-144.

Amiri, R., Weng, Q., Alimohammadi, A. and Alavipanah, S. K. (2009). Spatial–temporal dynamics of land surface temperature in relation to fractional vegetation cover and land use/cover in the Tabriz urban area. *Iran. Remote Sens. Environ., 113(12)*: 2606–2617.

Arnfield, A. J. (2003). Two Decade of Urban Climate Research. A Review of Turbulence Exchange of Energy and Water and the Urban Heat Island. *International Journal of Climatology, 23: 1-26.*

Avis, W. (2019). *Urban Expansion in Nigeria*. K4D Helpdesk Report 692. Brighton, UK: Institute of Development Studies.

Bagan, H., Takeuchi, W., Kinoshita, T., Bao, Y. and Yamagata, Y. (2010). Land cover classification and change analysis in the Horqin sandy land from 1975 to 2007. *IEEE J Sel Top Appl Earth Obs Remote Sens., 3(2):* 168–177.

Bharatkar, P. S. and Patel R. (2013). Approach to Accuracy Assessment for RS Image Classification Techniques. *International Journal of Scientific & Engineering Research*, 4(12): 79-86. ISSN 2229-5518.

Chander, G., Markham, B. L. and Helder, D. L. (2009). Summary of current radiometric calibration coefficients for Landsat MSS, TM, ETM+, and EO-1 ALI sensors. *Remote Sens. Environ., 113(5)*, 893–903.

Chen, Q., Ren, J., Li, Z. and Ni, C. (2009). Urban Heat Island Effect Research in Chengdu City Based on MODIS Data. Proceedings of the 3rd International Conference on Bioinformatics and Biomedical Engineering (ICBBE), Beijing, China, 11–13 June 2009; pp. 1-5.

Chen, X. L., Zhao, H. M., Li, P. X. and Yin, Z. Y. (2006). Remote sensing image-based analysis of the relationship between urban heat island and land use/cover changes. *Remote Sens. Environ., 104(2):* 133–146.

Egunjobi, L. (1999). *Our Gasping Cities,* An Inaugural Lecture delivered at the University of Ibadan on Thursday, 21 October 1999.

Egunjobi, L. (2002). Planning the Nigerian Cities for Better Quality of Life. In *Environment, Physical Planning and Development in Nigeria*, Onakomaiya, S. O., Oyesiku, O. O., Eds.; Department of Geography and Regional Planning, Olabisi Onabanjo University: Ago-Iwoye, Nigeria, 2002, pp. 89-107.

Igor, O. and Vanessa da Silva, B. B. (2012). A Quantitative Approach for Analysing the Relationship between Urban Heat Islands and Land Cover. *Journal of Remote Sensing, 4*: 3596-3618. doi:10.3390/rs4113596, ISSN 2072-4292.

Isioye, O. A., Akomolafe E. A., Abubakar A. Z., Aliyu O. A. and Maiwayo, T. (2019). Geospatial Analysis of Urban Heat Island over Bauchi Metropolis and its Environs. Proceedings of the 1st International Conference of Engineering and Environmental Sciences (ICEES), Osun State University (UNIOSUN), Osogbo, Nigeria, 5-7 November 2019; pp. 655-669.

Jhaldiyal, A. (2015). *Automatic Estimation of Urban Roughness Parameters for Microclimatic Analysis*. (Master's thesis, Urban and Regional Studies Department, Indian Institute of Remote Sensing (IIRS), Dehradun, India). Retrieved from https://www.iirs.gov.in/iirs/sites/default/files/StudentThesis/ALOK_MTech_2013-15.pdf

Kalnay, E. and Cai, M. (2003). Impact of Urbanization and Land-Use Change on Climate. *Nature, 423*(*6939*): 528−531.

Kikegawa, Y., Genchi, Y., Kendo, H. and Hanaki, K. (2006). Impact of City Block-Scale Countermeasures against Urban Heat Island Phenomena upon a Building Energy Consumption for Air Conditioning. *Journal of Applied Energy, 83:* 649-668.

Kumar, K. S., Bhaskar, P. U. and Padmakumarı, K. (2012). Estimation of land surface temperature to study urban heat island effect using Landsat ETM+ image. *Int J Eng Sci Technol (IJEST), 4(2):* 771–778.

Landsat Project Science Office. (2002). Landsat 7 Science Data user's Handbook.. Available online: http://ltpwww.gsfc.nasa.gov/IAS/handbook/handbook_toc.html (accessed 13 May 2018).

Landsat Project Science Office. (2016). Landsat 8 science data user's handbook. Available online: https://landsat.usgs.gov/documents/Landsat8DataUsersHandbook.pdf (accessed 13 May 2018).

Li, X., Zhou, W., Ouyang, Z., Xu, W. and Zheng, H. (2012). Spatial pattern of greenspace affects land surface temperature: evidence from the heavily urbanized Beijing metropolitan area, China. *Landscape Ecol., 27(6):* 887–898.

Nanzip, B. N. (2020). Jos City: Location, History, Urban Growth and Climate. Available online: https://www.jotscroll.com/forums/3/posts/144/jos-location-history-urban-growth-and-climate.html (accessed on 15 June 2020).

Oke, T. R. (1982). The energetic basis of the urban heat island. *Quarterly Journal of the Royal Meteorological Society***,** *108:* 1-24.

Olujimi, J. (2009). Evolving a Planning Strategy for Managing Urban Sprawl in Nigeria. *Journal of Human Ecology, 25* (3): 201-208. DOI: 10.1080/09709274.2009.11906156

Osborn, T. J., Wallace, C. J., Harris, I. C. and Melvin, T. M. (2016). Pattern scaling using ClimGen: monthly-resolution future climate scenarios including changes in the variability of precipitation. *Climatic Change, 134:* 353-369. https://dx.doi.org/10.1007/s10584-015-1509-9

Seifolddini, F. and Mansourian, H. (2014). Spatial-Temporal Pattern of Urban Growth in Tehran Megapole. *Journal of Geography and Geology, 6*(1).

Song, C., Woodcok, C. E., Seto, K. C., Lenney, M. P. and Macomber, S.A. (2001). Classification and Change Detection Using Landsat TM Data: When and How to Correct Atmospheric Effects. *Remote Sensing of Environment, 75:* 230-244.

Sun, Q., Wu, Z. and Tan, J. (2012). The relationship between land surface temperature and land use/land cover in Guangzhou, China. *Environ. Earth Sci. 65* (6), 1687–1694.

Ujoh, F., Kwabe, I. D. and Ifatimehin,O. O. (2010). Understanding Urban Sprawl in the Federal Capital City, Abuja: Towards Sustainable Urbanization in Nigeria. *Journal of Geography and Regional Planning, 3* (5): 106-113. Available online: http://www.academicjournals.org/JGRP

United Nations (UN) Department of Economic and Social Affairs, Population Division (2019). World Population Prospects 2019. Available online: https://population.un.org/wpp/.

USGS. (2017). What Are the Band Designation for Landsat Satellite? 2017. Available online: https://www.usgs.gov/faqs/what-are-band-designations-landsat-satellites-0?qt-news_science_products=7#qt-news_science_product (accessed 4 June 2018).

Vieira, S. M., Kaymak, U. and Sousa, J. M. C. (2010). Cohen Kappa Coefficient as a performance Measure for Feature Selection. In Proceedings of 2010 IEEE International Conference. doi: 978-1-4244-8126-2/10.

Voogt, J. A. and Oke, T. R. (2003). Thermal remote sensing of urban climates. *Remote Sensing of Environment, 86:* 370-84.

World Bank Group (2020). Climate Change Knowledge Portal: Nigeria. Available online: https://climateknowledgeportal.worldbank.org/country/nigeria/climate-data-projections.

Yuan, F., Sawaya, K. E., Loeffelholz, B. C. and Bauer, M. E. (2005). Land cover classification and change analysis of the twin cities (Minnesota) metropolitan area by multitemporal Landsat remote sensing. *Remote Sens. Environ.*, *98*: 317–328.

Zha, Y., Gao, J. and Ni, S. (2005). Use of normalized difference built-up index in automatically mapping urban areas from TM imagery. *International Journal of Remote Sensing, 24:* 583–594.

Zhou, L., Dickinson, R. E., Tian, Y., Fang, J., Li, Q., Kaufmann, R. K., Tucker, C. J., and Myneni, R. B. (2004). Evidence for a significant urbanization effect on climate in China. *Proc. Natl. Acad. Sci. USA, 101:* 9540–9544. doi:10.1073/pnas.0400357101.